Journal of Thermal Analysis and Calorimetry (2021) 144:1253–1270
https://doi.org/10.1007/s10973-020-09636-5

Optimization of heat transfer properties on ferrofluid flow over a stretching sheet in the presence of static magnetic field

Anupam Bhandari[1] · Akmal Husain[1]

Received: 11 November 2019 / Accepted: 24 March 2020 / Published online: 9 April 2020

Abstract

The main emphasis of the present research is to investigate the composite effects of magnetization force and rotational viscosity on two-dimensional ferrohydrodynamic non-conducting nanofluid flow over a stretching sheet under the influence of the stationary magnetic field. Microrotation of magnetic fluid and rotation of nanoparticles are also considered. Shliomis model is used in the problem formulation, and then the similarity transformation is applied to transform partial differential equations into a set of nonlinear-coupled ordinary differential equations in dimensionless form. Transformed nonlinear-coupled differential equations are solved through the finite element method using COMSOL Multiphysics under the mathematical modeling. Results for velocity distribution, temperature distribution, concentration distribution and angular velocity distribution are obtained after considering the effects of Maxwell parameter, ferromagnetic interaction number, thermal Grashof number, solutal Grashof number, Brownian motion parameter, thermophoresis number, chemical reaction parameter, radiation absorption coefficient, heat generation/absorption parameter, Prandtl number and Schmidt number in the flow. It has been observed that magnetic energy transforms into kinetic energy, thermal boundary layer and concentration boundary layer in the presence of considered physical parameters.

Keywords Magnetic dipole · Stretching sheet · Ferrofluid · Heat and mass transfer

List of symbols

A	Positive constant
a	Distance
c	Stretching rate (s^{-1})
c_p	Specific heat at constant pressure $\left(J\,kg^{-1}\,K^{-1}\right)$
C	Concentration of the fluid inside the boundary layer ($kg\,m^{-3}$)
C_∞	Concentration of the fluid outside the boundary layer ($kg\,m^{-3}$)
C_w	Species concentration at the wall of the temperature ($kg\,m^{-3}$)
C_{fx}	Skin friction coefficient
D_B	Brownian diffusion coefficient
D_T	Thermophoresis coefficient
f	Dimensionless stream function
Gr	Thermal Grashof number
Gm	Solutal Grashof number
g	Dimensionless angular velocity
g_0	Acceleration due to gravity (ms^{-2})
I	Sum of the particles moment of inertia ($kg\,m^2$)
H	Magnetic field intensity ($A\,m^{-1}$)
j	Micro-inertia per unit mass (m^2)
k	Thermal conductivity ($W\,m^{-1}\,K^{-1}$)
K	Material parameter
K^a	Pyromagnetic coefficient
K_1	Chemical reaction parameter
l	Characteristic length
M	Magnetization ($A\,m^{-1}$)
m_1	Effective magnetic parameter
Nb	Brownian motion parameter
Nt	Thermophoresis parameter
Nu_x	Nusselt number
Pr	Prandtl number
Q_0	Heat absorption coefficient
Q_1'	Radiation absorption coefficient
Q_1	Radiation absorption coefficient
q_w	Heat transfer rate (W)
Re_x	Local Reynolds number
S	Suction parameter

✉ Anupam Bhandari
pankaj.anupam6@gmail.com

[1] Department of Mathematics, School of Engineering, University of Petroleum and Energy Studies (UPES), Energy Acres Building, Bidholi, Dehra Dun, Uttarakhand 248007, India

Sh_x	Sherwood number
Sc	Schmidt number
T	Temperature (K)
T_w	Wall temperature (K)
T_c	Curie temperature (K)
T_∞	Temperature outside the boundary layer (K)
u	Velocity component along the sheet (ms^{-1})
v	Velocity component normal to the sheet (ms^{-1})
x	Coordinate along sheet (m)
y	Coordinate normal to the sheet (m)
α_1	Dimensionless distance from origin to dipole
β	Ferromagnetic interaction number
γ_1	Maxwell parameter
γ	Chemical reaction parameter
γ_0	Magnetic field strength ($A\ m^{-1}$)
γ_F	Spin gradient viscosity
λ	Viscous dissipation parameter
λ_1	Relaxation time
φ	Dimensionless concentration
Φ_1	Volume fraction
ε	Dimensionless curie temperature
η	Dimensionless coordinate
θ	Dimensionless temperature
λ	Viscous dissipation parameter
μ	Dynamic viscosity $\left(kg\,m^{-1}\,s^{-1}\right)$
ν	Kinematic viscosity $\left(m^{-2}\,s^{-1}\right)$
μ_0	Permeability
ρ	Density $\left(kg\,m^{-3}\right)$
ξ	Dimensionless coordinate
χ	Heat absorption parameter
τ_s	Rotational relaxation time $\left(s^{-1}\right)$
Θ	Magnetic potential ($A\ m^{-1}$)
ψ	Stream function $\left(m^2\,s^{-1}\right)$
$\left(\rho c_p\right)_p$	Heat capacitance of nanoparticles
Ω	Angular velocity (rad s^{-1})
Ω_p	Angular velocity of particles (rad s^{-1})

Introduction

Ferrofluids are suspensions of nanometer-sized magnetic particles in a suitable carrier liquid. It is synthesized through a chemical process. Ferrofluids is a kind fluid, which works in the zero gravity regions. Ferrofluids can be used in cooling of power electronics, computers and solar cells. Magnetic fluid has been extensively used in varieties of application in leak free seals, lubricants, density separation, ink jet printers, tunable heat transfer fluid, diagnostics in medicine, for heat transport of solar heat, etc. Due to low thermal conductivity of traditional fluid, nanofluid has been used recently in heat transfer applications. Nowadays, most of the heat transfer research has been carried out on Magnetohydrodynamic (MHD) nanofluid flow. MHD is concerned with the study of the interaction between magnetic fields and fluid conductors of electricity. The body force acting on the fluid is the Lorentz force that arises when electric current flows at an angle to the direction of an impressed magnetic field. In the current study, heat transfer analysis has been carried out on ferrohydrodynamic (FHD) nanofluid flow. FHD deals with the mechanics of fluid motion influenced by strong forces of magnetic polarization and there needS to be no electric current flowing in the fluid. Magnetization force works on throughout the volume of the fluid. It changes the viscosity of the magnetic fluid also. In the presence of stationary magnetic field, it creates additional resistance on FHD nanofluid flow. This additional resistance creates rotational viscosity of ferromagnetic fluid. Rotational viscosity depends on the strength of the magnetic field.

Rosensweig has demonstrated that due to the absence of current density in ferrofluid, the magnetic body force per unit volume is $\mu_0(\boldsymbol{M}.\nabla)\boldsymbol{H}$ where μ_0 is the magnetic permeability, $\boldsymbol{M}$ is the magnetization and $\boldsymbol{H}$ is the magnetic field intensity [1]. Boundary layer flow of heated ferrofluid along a flat plat and stagnation point flow with variable magnetic field have been investigated [2]. Viscous and non-conducting flow of magnetic fluid over a stretching sheet has been investigated [3]. Heat transfer Jeffery ferrofluid past a lineally stretching sheet by considering the effect of magnetic dipole has been studied [4]. Heat transfer analysis on ferrofluid flow in a miniature channel in the presence of oscillating and uniform magnetic field has been studied [5]. Electrokinetic flow of nanofluid through a porous microtube in the presence of external magnetic field has been studied [6]. Heat transfer on different types of nanofluid has been investigated by finite element method [7]. A brief overview on nanofluid research and heat transfer enhancement has been published in the review article [8]. Convective heat transfer enhancement in nanofluid has been studied [9]. Control volume finite element has been used to study the impact of Coulomb force, entropy analysis and heat transfer analysis on ferromagnetic nanofluid flow [10–12]. The behavior of water-based nanofluid in the presence of nonuniform magnetic field has been analyzed numerically [13]. A numerical study presented for ferrofluid in a porous elliptical enclosure [14].

Dynamic viscosity plays an important role in the heat transfer analysis [15]. Convective heat transfer on nanofluid flow has been studied with control finite volume method [16]. Heat transfer characteristics of nanofluid over a inclined vertical plate have been investigated [17]. MHD flow over a stretching sheet has been considered, and different types of stretching have been used by the researchers [18–21]. Convective heat transfer on magnetic nanofluid with a sinusoidal hot wall has been investigated, and homotopy analysis has been used in the solution of nonlinear-coupled differential equations [22, 23]. Buoyancy and heat transfer characteristics have been investigated analytically [24]. A model for studying chemical reaction on two-dimensional ferrofluid flow due to a stretching sheet has been constructed [25, 26]. Decreasing the coil diameter increases the heat transfer on ferrofluid through a helical tube [27]. Three-dimensional flow of nanofluid containing ferrous nanoparticles over a variable sheet in a slip flow regime have been investigated [28]. Thermomagnetic convection of a ferrofluid flow around a vertical current-carrying wire has been studied [29].

Boundary layer flow of ferrofluid over a stretching surface with the influence of magnetic has been studied [30]. Effect of magnetic dipole on Williamson ferrofluid over a stretching surface has been solved with the help of shooting method [31]. Finite element method has been used to solve a set of nonlinear partial differential equations [32]. Field-dependent viscosity effects on ferrofluid flow in the presence of a disk have studied in the presence of alternating magnetic field and stationary magnetic field [33, 34]. Radiation effects on two-dimensional ferrofluid flow over a stretching surface has been investigated [35]. Effect of magnetic field location on heat transfer has been studied [36].

From above the literature survey, most of the research work has been carried out on the MHD nanofluid flow. However, there are few numbers of research papers, which are published on FHD nanofluid flow. The above literature survey motivates toward the FHD nanofluid flow and its heat transfer characteristics. In the present problem, the two-dimensional incompressible viscous flow of ferrofluid over a stretching sheet has been considered. Rotation of the particles in the ferrofluid is also included in the calculations. Thermal and concentration buoyancy effects, heat absorption and radiation effects, chemical reaction effects, Brownian motion effects, thermophoresis effects and magnetization force effects have been considered. A system of partial differential equation has been transformed to ordinary nonlinear-coupled differential equations. A set of nonlinear-coupled differential equations is solved through finite element method using COMSOL Multiphysics.

Mathematical formulation

A schematic diagram for electrically non-conducting, steady and an incompressible two-dimensional ferrohydrodynamic (FHD) nanofluid flow over a linear stretching sheet is presented in Fig. 1. Stretching in the sheet is along x axis with the velocity u_w due to the force exerted on the sheet $y = 0$ and y axis is taken normal to the sheet. A magnetic dipole is kept in the center of the y axis and a unit distance from the sheet. Stretching on the sheet is proportional to the distance from the origin. Wall temperature is assumed as T_w. Curie temperature is denoted

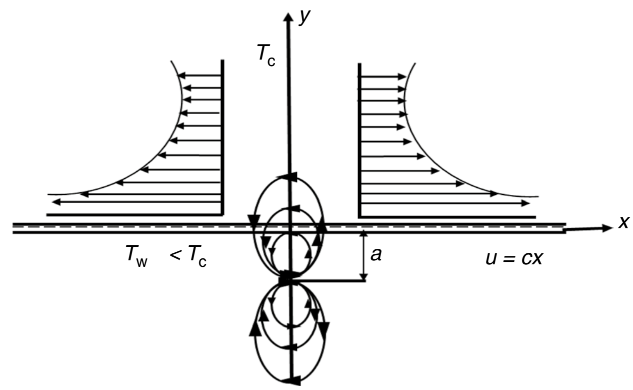

Fig. 1 Geometry of flow configuration. Circles represent magnetic dipole

by T_c, while ambient temperature is $T_\infty = T_c$. Magnetic effects become zero beyond the Curie temperature. The angular velocity is zero at the surface of the sheet as well as far away from the sheet. Microrotation of the fluid and rotation of the particle are also considered. The motion of the ferrofluid over a stretching sheet is caused by moving sheet. Rotation of the ferrofluid and nanoparticles in the fluid is also considered.

The governing equations for this type of flow based on Shliomis model are as follows [37]:

The equation of continuity

$$\frac{\partial u}{\partial x} + \frac{\partial v}{\partial y} = 0 \tag{1}$$

The equation of motion

$$u\frac{\partial u}{\partial x} + v\frac{\partial u}{\partial y} + \lambda_1\left(u^2\frac{\partial^2 u}{\partial x^2} + v^2\frac{\partial^2 u}{\partial y^2} + 2uv\frac{\partial^2 u}{\partial x\partial y}\right)$$
$$= \frac{\mu_0}{\varrho}M\frac{\partial H}{\partial x} + v\frac{\partial^2 u}{\partial y^2} + \frac{k}{\rho}\frac{\partial \Omega}{\partial y}$$
$$+ g_0\beta_1(T - T_\infty) + g_0\beta_2(C - C_\infty) + \frac{I}{2\tau_s}\left(\frac{\partial \Omega_p}{\partial y} - \frac{\partial \Omega}{\partial y}\right) \tag{2}$$

The energy equation

$$u\frac{\partial T}{\partial x} + v\frac{\partial T}{\partial y} + \frac{\mu_0 T}{\rho C_p}\frac{\partial M}{\partial T}\left(u\frac{\partial H}{\partial x} + v\frac{\partial H}{\partial y}\right)$$
$$= \frac{k}{\rho C_p}\frac{\partial^2 T}{\partial y^2} + \frac{k}{\rho C_p}\left[\mu\left(\frac{\partial u}{\partial y}\right)^2 + 2\mu\left(\frac{\partial v}{\partial y}\right)^2\right]$$
$$+ \frac{(\rho c_p)_p}{\rho c_p}\left[D_B\frac{\partial C}{\partial y}\frac{\partial T}{\partial y} + \frac{D_T}{T_\infty}\left(\frac{\partial T}{\partial y}\right)^2\right]$$
$$+ \frac{(\rho c_p)_p}{\rho c_p}D_B\frac{\partial^2 C}{\partial y^2} - \frac{Q_0}{\rho c_p}(T - T_\infty) + Q_1'(C - C_\infty) \tag{3}$$

The equation of concentration

$$u\frac{\partial C}{\partial x}+v\frac{\partial C}{\partial y}=D_{\mathrm{B}}\frac{\partial^2 C}{\partial y^2}++\frac{D_{\mathrm{T}}}{T_\infty}\frac{\partial^2 T}{\partial y^2}-K_1\left(C-C_\infty\right) \quad (4)$$

The equation of angular momentum

$$u\frac{\partial \Omega}{\partial x}+v\frac{\partial \Omega}{\partial y}=\frac{\gamma_{\mathrm{F}}}{j\rho}\frac{\partial^2 \Omega}{\partial y^2}+\frac{k}{j\rho}\left(2\Omega+\frac{\partial u}{\partial y}\right) \quad (5)$$

The boundary conditions for described flow are as follows:

$$y=0: \quad u=v_{\mathrm{w}}=cx; \quad v=0; \quad T=T_{\mathrm{w}}=T_{\mathrm{E}}-A\left(\frac{x}{l}\right)^2; \quad C=C_{\mathrm{w}}; \quad \Omega=0 \quad (6)$$

$$y\to\infty: \quad u=0; \quad T=T_\infty; \quad C=C_\infty; \quad \Omega=0 \quad (7)$$

The expression $\frac{I}{2\tau_{\mathrm{s}}}\left(\frac{\partial\Omega_{\mathrm{p}}}{\partial y}-\frac{\partial\Omega}{\partial y}\right)=\frac{3}{2}\Phi_1 m_1 v\frac{\partial^2 u}{\partial y^2}$ viscous force due to rotation of the magnetic fluid [33, 38]. $l=\sqrt{\frac{v}{c}}$ is the characteristic length.

There is no current density in ferrofluid. The considered fluid motion is controlled by the applied magnetic field as shown in Fig. 1. The scalar potential for the applied magnetic field is:

$$\Theta=\frac{\gamma_0}{2\pi}\left\{\frac{x}{x^2+(y+a)^2}\right\} \quad (8)$$

The components of magnetic field intensity H_{x} and H_{y} along x and y axes can be expressed as:

$$H_{\mathrm{x}}=-\frac{\partial\Theta}{\partial x}=\frac{\gamma_0}{2\pi}\left[\frac{x^2-(y+a)^2}{\left\{x^2+(y+a)^2\right\}^2}\right] \quad (9)$$

$$H_{\mathrm{y}}=-\frac{\partial\Theta}{\partial y}=\frac{\gamma_0}{2\pi}\left[\frac{2x(y+a)}{\left\{x^2+(y+a)^2\right\}^2}\right] \quad (10)$$

The resultant magnitude of the magnetic field intensity is:

$$H=\left[\left(\frac{\partial\Theta}{\partial x}\right)^2+\left(\frac{\partial\Theta}{\partial y}\right)^2\right]^{\frac{1}{2}} \quad (11)$$

The gradient of magnitude of the magnetic field intensity along x and y axes are as follows:

$$\frac{\partial H}{\partial x}=\frac{\gamma_0}{2\pi}\left\{\frac{2x}{(y+a)^4}\right\} \quad (12)$$

$$\frac{\partial H}{\partial y}=\frac{\gamma_0}{2\pi}\left\{\frac{-2}{(y+a)^3}+\frac{4x^2}{(y+a)^5}\right\} \quad (13)$$

Magnetization is considered as a linear function of temperature as:

$$M=K^{\mathrm{a}}\left(T_{\mathrm{c}}-T\right) \quad (14)$$

Fluid temperature is different from Curie temperature. Once ferrofluid approaches to Curie temperature, there is no furthermore magnetization. It is the situation when all the magnetic particles aligned in the direction of applied magnetic field.

Solution procedure

Using the following similarity transformation, the described model in the above section has now been converted into dimensionless from

$$\psi=\frac{\mu}{\rho}\xi f(\eta); \quad \theta=\frac{T_{\mathrm{c}}-T}{T_{\mathrm{c}}-T_{\mathrm{w}}}=\theta_1(\eta)+\xi^2\theta_2(\eta); \quad \varphi=\frac{C-C_\infty}{C_{\mathrm{w}}-C_\infty}; \quad \Omega=\sqrt{\frac{c^3}{v}}xg(\eta) \quad (15)$$

$$T_{\mathrm{c}}-T_{\mathrm{w}}=A\left(\frac{x}{l}\right)^2; \quad \xi=\sqrt{cv}x; \quad \eta=\sqrt{cv}y \quad (16)$$

The velocity components u and v are related to the stream function as:

$$u=\frac{\partial\psi}{\partial y}=cxf'(\eta); \quad v=-\frac{\partial\psi}{\partial x}=-\sqrt{cv}f(\eta) \quad (17)$$

Here, prime represents the differentiation with respect to η. Using Eqs. (15)–(17) and equating the coefficients of equal powers of ξ up to ξ^2, the equation of motion of motion, the energy equation, the concentration equation and the equation of angular momentum transform into a set of nonlinear-coupled differential equations as:

$$\left(1+\frac{3}{2}\phi_1 m_1\right)\frac{\mathrm{d}^3 f}{\mathrm{d}\eta^3}-\gamma_1 f^2\frac{\mathrm{d}^3 f}{\mathrm{d}\eta^3}-\left\{\left(\frac{\mathrm{d}f}{\mathrm{d}\eta}\right)^2-f\frac{\mathrm{d}^2 f}{\mathrm{d}\eta^2}\right\}+2\gamma_1 f\frac{\mathrm{d}f}{\mathrm{d}\eta}\frac{\mathrm{d}^2 f}{\mathrm{d}\eta^2}-\frac{2\beta}{\left(\eta+\alpha_1\right)^4}\theta_1+K\frac{\mathrm{d}g}{\mathrm{d}\eta}-\mathrm{Gr}\theta_1-\mathrm{Gm}\varphi=0 \quad (18)$$

$$\frac{\mathrm{d}^2\theta_1}{\mathrm{d}\eta^2}+\mathrm{Pr}\left(f\frac{\mathrm{d}\theta_1}{\mathrm{d}\eta}-2\frac{\mathrm{d}f}{\mathrm{d}\eta}\theta_1\right)+\frac{2\lambda\beta\left(\theta_1-\varepsilon\right)f}{\left(\eta+\alpha_1\right)^3}-2\lambda\left(\frac{\mathrm{d}f}{\mathrm{d}\eta}\right)^2-\mathrm{Nb}\frac{\mathrm{d}^2\varphi}{\mathrm{d}\eta^2}+\mathrm{Nb}\frac{\mathrm{d}\theta_1}{\mathrm{d}\eta}\frac{\mathrm{d}\varphi}{\mathrm{d}\eta}+\mathrm{Nt}\left(\frac{\mathrm{d}\theta_1}{\mathrm{d}\eta}\right)^2-\chi\theta_1+Q_1\varphi=0 \quad (19)$$

$$\frac{d^2\theta_2}{d\eta^2} - \Pr\left(4\frac{df}{d\eta}\theta_2 - f\frac{d\theta_2}{d\eta}\right) + \frac{2\lambda\beta f\theta_2}{(\eta+\alpha_1)^3} - \lambda\beta(\theta_1-\varepsilon)\left\{\frac{2\frac{df}{d\eta}}{(\eta+\alpha_1)^4} + \frac{4f}{(\eta+\alpha_1)^5}\right\} - \lambda\left(\frac{df}{d\eta}\right)^2 + \text{Nb}\frac{d\theta_2}{d\eta}\frac{d\varphi}{d\eta} + \text{Nt}\left(\frac{d\theta_2}{d\eta}\right)^2 - \chi\theta_2 + Q_1\varphi = 0 \quad (20)$$

$$\frac{d^2\varphi}{d\eta^2} + \text{Sc}\,f\frac{d\varphi}{d\eta} - \text{Sc}\gamma\varphi + \frac{\text{Nt}}{\text{Nb}}\frac{d^2\theta_2}{d\eta^2} = 0 \quad (21)$$

$$\left(1+\frac{K}{2}\right)\frac{d^2g}{d\eta^2} + f\frac{dg}{d\eta} - \frac{df}{d\eta}g - K\left(2g + \frac{d^2f}{d\eta^2}\right) = 0 \quad (22)$$

The transformed boundary conditions from Eqs. (6) and (7) are as follows:

$$f(0) = S;\quad f'(0) = 0;\quad \theta_1(0) = 1;\quad \theta_2(0) = 0;\quad \varphi(0) = 1;\quad g(0) = 0 \quad (23)$$

$$f'(\infty) = 0;\quad \theta_1(\infty) = 0;\quad \theta_2(\infty) = 0;\quad \varphi(\infty) = 0;\quad g(\infty) = 0 \quad (24)$$

The dimensionless quantities are presented as follows:

$$\beta = \frac{\gamma_0\rho}{2\pi\mu^2}\mu_0K^a(T_c - T_w);\quad \gamma_1 = \lambda_1 c;$$
$$\lambda = \frac{c\mu^2}{\rho k(T_c - T_w)};\ \Pr = \frac{\mu c_p}{k};\quad \alpha_1 = \sqrt{\left(\frac{c\rho}{\mu}\right)}a;$$
$$\varepsilon = \frac{T_c}{T_c - T_w},\ \text{Sc} = \frac{\mu}{\rho D};\quad K = \frac{k}{\mu};\quad \text{Gr} = \frac{\mu g_0\beta_1(T_w - T_c)}{\rho\nu^3};$$
$$\text{Gm} = \frac{\mu g_0\beta_2(C_w - C_\infty)}{\rho\nu^3};\quad Q_1 = \frac{\mu Q_1'(C_w - C_\infty)}{\rho\nu^2(T_w - T_c)};$$
$$\chi = \frac{Q_0\mu}{\rho^2c_p\nu^2},\ \gamma = \frac{K_1\mu}{\rho\nu^2};\quad \text{Nb} = \frac{(\rho c_p)_p D_B(C_w - C_\infty)}{\rho c_p\nu};$$
$$\text{Nt} = \frac{(\rho c_p)_p D_T(T_w - T_c)}{\rho c_p\nu T_c} \quad (25)$$

Equations (18)–(22) with the help of Eqs. (23) and (24) are solved using finite element method in COMSOL Multiphysics. For use system of differential equation tool in COMSOL, these equations are converted to second order differential equations as:

$$f = p;\quad \frac{df}{d\eta} = q \quad (26)$$

$$\frac{dp}{d\eta} = q \quad (27)$$

$$\left(1+\frac{3}{2}\phi_1m_1\right)\frac{d^2q}{d\eta^2} - \gamma_1p^2\frac{d^2q}{d\eta^2} - \left\{q^2 - p\frac{dq}{d\eta}\right\} + 2\gamma_1pq\frac{dq}{d\eta} - \frac{2\beta}{(\eta+\alpha_1)^4}\theta_1 + K\frac{dg}{d\eta} - \text{Gr}\theta_1 - \text{Gm}\varphi = 0 \quad (28)$$

$$\frac{d^2\theta_1}{d\eta^2} + \Pr\left(p\frac{d\theta_1}{d\eta} - 2q\theta_1\right) + \frac{2\lambda\beta(\theta_1-\varepsilon)p}{(\eta+\alpha_1)^3} - 2\lambda q^2 - \text{Nb}\frac{E^2\varphi}{d\eta^2} + \text{Nb}\frac{d\theta_1}{d\eta}\frac{d\varphi}{d\eta} + \text{Nt}\left(\frac{d\theta_1}{d\eta}\right)^2 - \chi\theta_1 + Q_1\varphi = 0 \quad (29)$$

$$\frac{d^2\theta_2}{d\eta^2} - \Pr\left(4q\theta_2 - p\frac{d\theta_2}{d\eta}\right) + \frac{2\lambda\beta p\theta_2}{(\eta+\alpha_1)^3} - \lambda\beta(\theta_1-\varepsilon)\left\{\frac{2q}{(\eta+\alpha_1)^4} + \frac{4p}{(\eta+\alpha_1)^5}\right\} - \lambda q^2 + \text{Nb}\frac{d\theta_2}{d\eta}\frac{d\varphi}{d\eta} + \text{Nt}\left(\frac{d\theta_2}{d\eta}\right)^2 - \chi\theta_2 + Q_1\varphi = 0 \quad (30)$$

$$\frac{d^2\varphi}{d\eta^2} + \text{Sc}\,p\frac{d\varphi}{d\eta} - \text{Sc}\,\gamma\varphi + \frac{\text{Nt}}{\text{Nb}}\frac{d^2\theta_2}{d\eta^2} = 0 \quad (31)$$

$$\left(1+\frac{K}{2}\right)\frac{d^2g}{d\eta^2} + p\frac{dg}{d\eta} - qg - K\left(2g + \frac{dq}{d\eta}\right) = 0 \quad (32)$$

Dirichlet boundary conditions used to solve Eqs. (27)–(32) are as follows:

$$p(0) = S;\quad q(0) = 1;\quad \theta_1(0) = 1;\quad \theta_2(0) = 0;\quad \varphi(0) = 1;\quad g(0) = 0 \quad (33)$$

$$q(\infty) = 0;\quad \theta_1(\infty) = 0;\quad \theta_2(\infty) = 0;\quad \varphi(\infty) = 0;\quad g(\infty) = 0 \quad (34)$$

The physical quantities of practical interest are skin friction coefficient, heat transfer rate and Sherwood number, which can be expressed as:

$$C_{f_x} = -\frac{\tau_w}{\rho(cx)^2};\quad Nu_x = -\frac{xq_w}{k(T_c - T_w)};\quad Sh_x = \frac{xJ_w}{D_f(C_w - C_\infty)} \quad (35)$$

$$\tau_w = \mu(1+\gamma_1)\left(\frac{\partial u}{\partial y}\right)_{y=0};\quad q_w = -\left(\frac{\partial T}{\partial y}\right)_{y=0};\quad J_w = -D_f\left(\frac{\partial C}{\partial y}\right)_{y=0} \quad (36)$$

Using Eqs. (15)–(17), the above physical quantities can be written as:

$$C_f\sqrt{\mathrm{Re}_x} = -(1+\gamma_1)f'(0);\quad \frac{\mathrm{Nu}_x}{\sqrt{\mathrm{Re}_x}} = -\left\{\theta_1'(0) + \xi^2\theta_2'(0)\right\};\quad \frac{\mathrm{Sh}_x}{\sqrt{\mathrm{Re}_x}} = -\varphi'(0) \tag{37}$$

For modeling of Eqs. (26)–(34) in COMSOL Multiphysics, PDE interface has been used in the solution. The transformed differential equations are one-dimensional; therefore a line geometry has been drawn. In coefficient form PDE, Dirichlet boundary conditions are introduced in COMSOL. For solving this one-dimensional problem, the maximum element size in the solution is taken 0.001 and the minimum element size is 0.00008. Maximum element growth rate is 1.1. Resolution for narrow region is 1. For the coupling of the differential equations, nonlinear method has been selected as automatic Newton method; initial damping factor is taken 1. Minimum damping factor is selected 10^{-4}. Recovery damping factor is 0.75. Maximum number of iterations are selected 50. Residual factor is 1000. The error in the solution is of 10^{-7} order. The flowchart for the solution used in COMSOL is as follows:

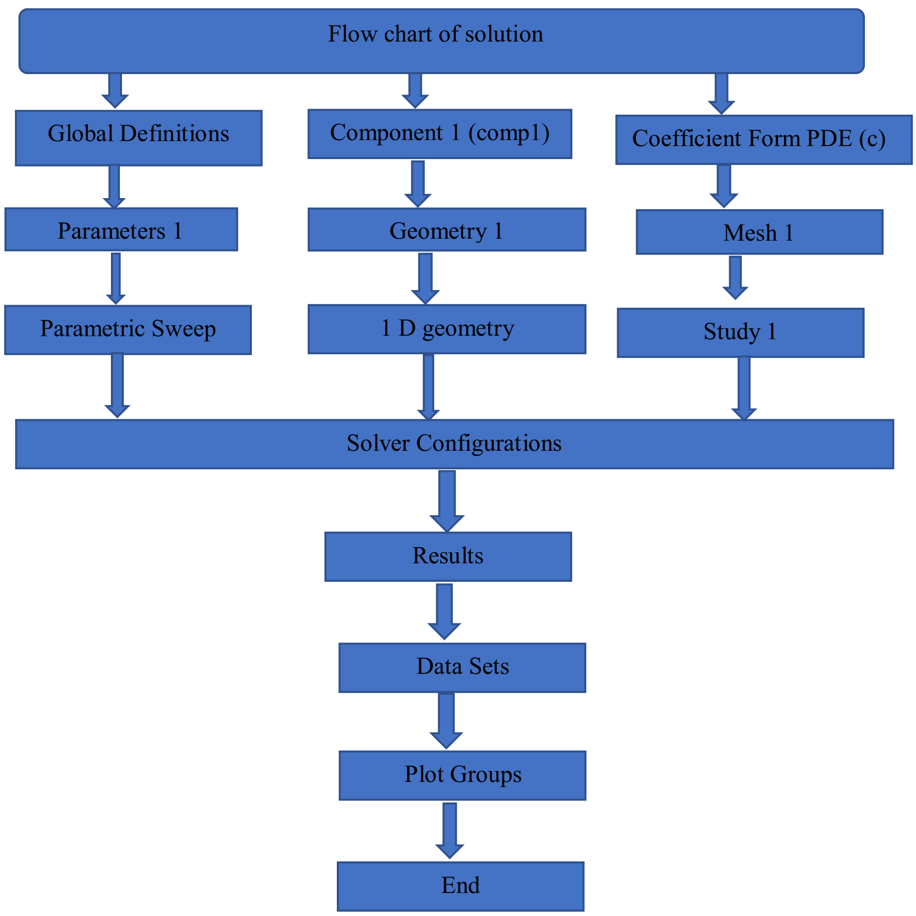

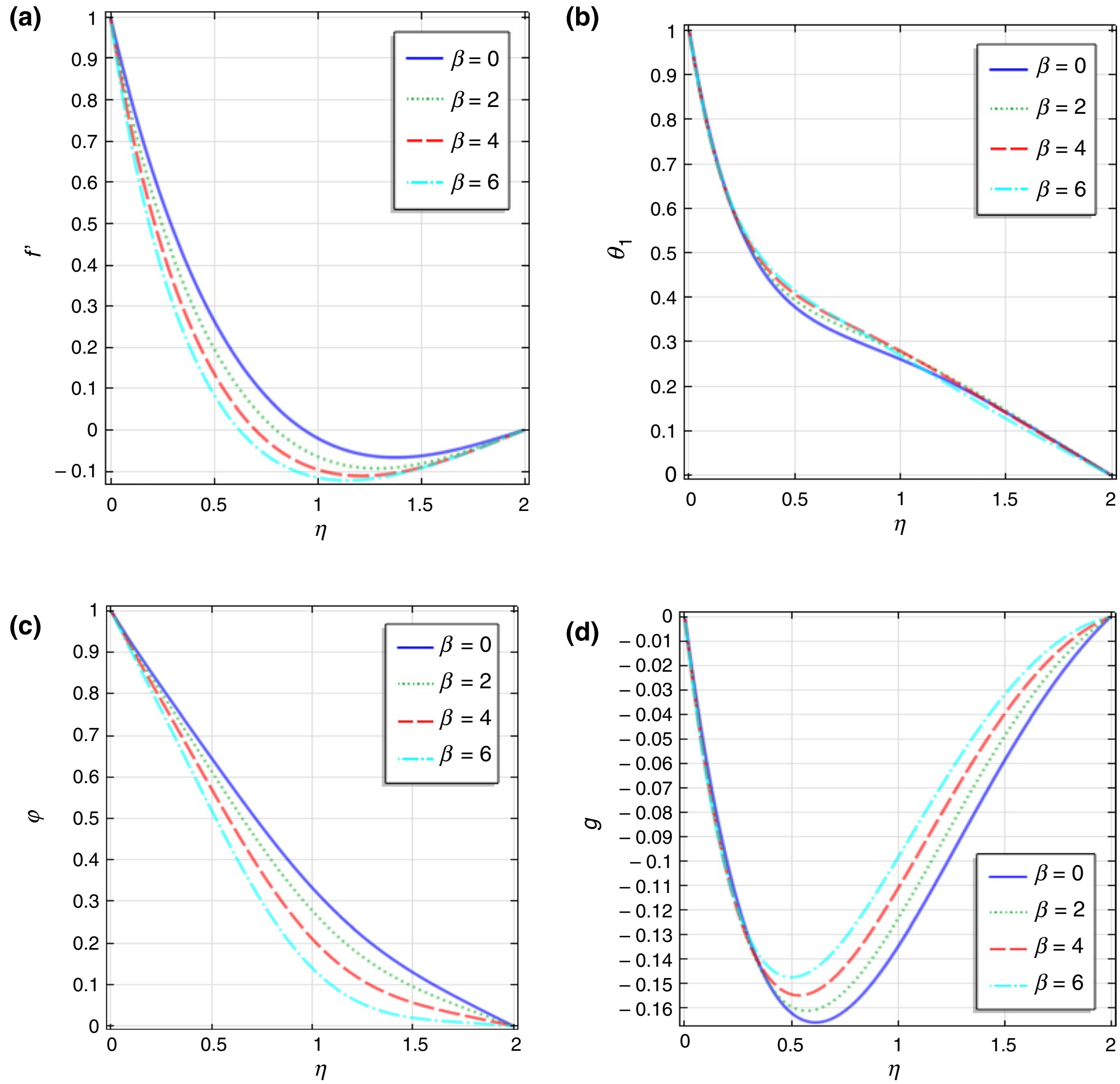

Fig. 2 **a** Velocity distribution, **b** concentration distribution, **c** concentration distribution, **d** angular velocity distribution for different values of β at $m_1 = 10, \phi_1 = 0.4, K = 0.2$, Gr = 2, Gm = 2, $\gamma_1 = 0.1, \alpha_1 = 1$, Pr = 10, $\lambda = 0.01$, $\varepsilon = 0.1$, Nb = 0.1, Nt = 0.1, $\chi = 2$, $Q_1 = 2$, Sc = 0.2, $S = 0.1$

Results and discussion

Results for velocity distributions (f'), temperature distributions (θ_1), concentration distributions (φ) and angular velocity distributions (g) are presented in graphical form for different values of Maxwell parameter (γ_1), ferromagnetic interaction number (β), thermal Grashof number (Gr), solutal Grashof number (Gm), Brownian motion parameter (Nb), thermophoresis number (Nt), chemical reaction parameter (γ), radiation absorption coefficient (Q_1), heat generation/absorption parameter (χ), Prandtl number (Pr) and Schmidt number (Sc). The default values of the parameters in the present work are considered as $m_1 = 0.4, \phi_1 = 0.4, \gamma_1 = 0.1$, $K = 0.2$, Gr = 2, Gm = 2, $\beta = 0.1, \alpha_1 = 1$, Pr = 10, $\lambda = 0.01$, $\varepsilon = 0.1$, Nb = 0.1, Nt = 0.1, $\chi = 2, Q_1 = 2$, Sc = 0.2, $\gamma = 2$. In the present study, viscous dissipation has been neglected. Therefore, at $\lambda = 0$ gives the trivial solution $\theta_2 = 0$.

Figure 2a–d represents the velocity, temperature, concentration and angular velocity distributions of different values of ferromagnetic interaction number. Increasing values of ferromagnetic interaction number decreases the velocity distribution and concentration distribution. Increasing the values of β, temperature distribution increases in the fluid. Ferromagnetic interaction number impedes the rotation of the particles in the fluid. These results indicate that magnetization force creates an additional resistance on the flow which reduces the velocity in the flow. There are magnetic

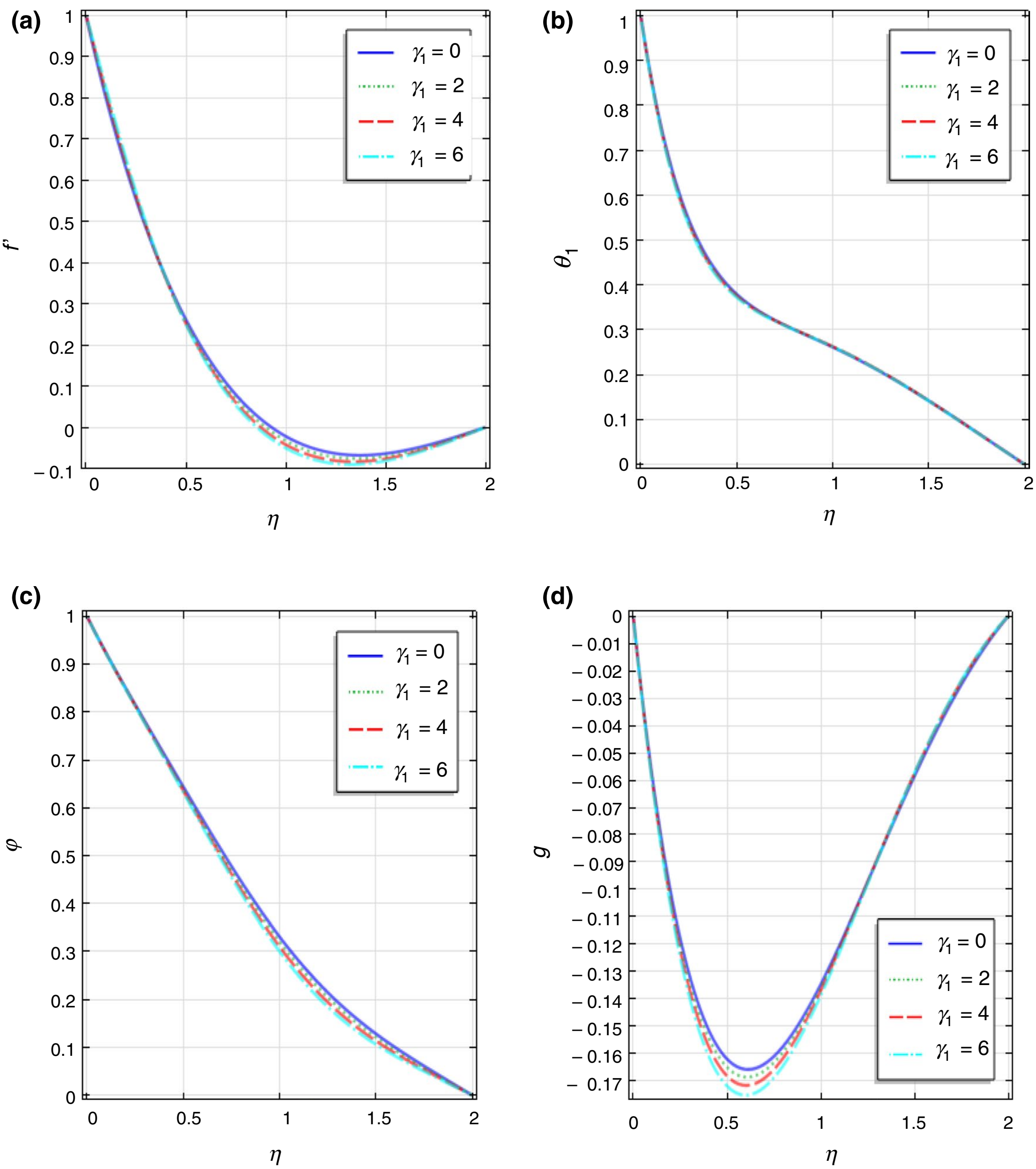

Fig. 3 **a** Velocity distribution, **b** temperature distribution, **c** concentration distribution, **d** angular velocity distribution for different values of γ_1 at $m_1 = 10, \phi_1 = 0.4, K = 0.2, \mathrm{Gr} = 2, \mathrm{Gm} = 2, \beta = 0.1, \alpha_1 = 1, \mathrm{Pr} = 10, \lambda = 0.01, \epsilon = 0.1, \mathrm{Nb} = 0.1, \mathrm{Nt} = 0.1, \chi = 2, Q_1 = 2, \mathrm{Sc} = 0.2, S = 0.1$

nanoparticles in ferrofluid which aligned in the direction of the applied magnetic field. This intervention in the flow decreases the velocity distribution. Figure 3a–d shows the velocity, temperature, concentration and angular velocity distributions, respectively, for different values of Maxwell parameter γ_1. Increasing the values of γ_1, the velocity distribution decreases. Figure 3d shows that the angular velocity distribution of the fluid increases for increasing values of Maxwell parameter. Maxwell parameter favors the rotation of the particle in the fluid. There is no significant impact of γ_1 on the temperature distribution. However, increasing γ_1 decreases the concentration distribution.

Figure 4a–d shows the velocity, temperature, concentration and angular velocity distribution for different values

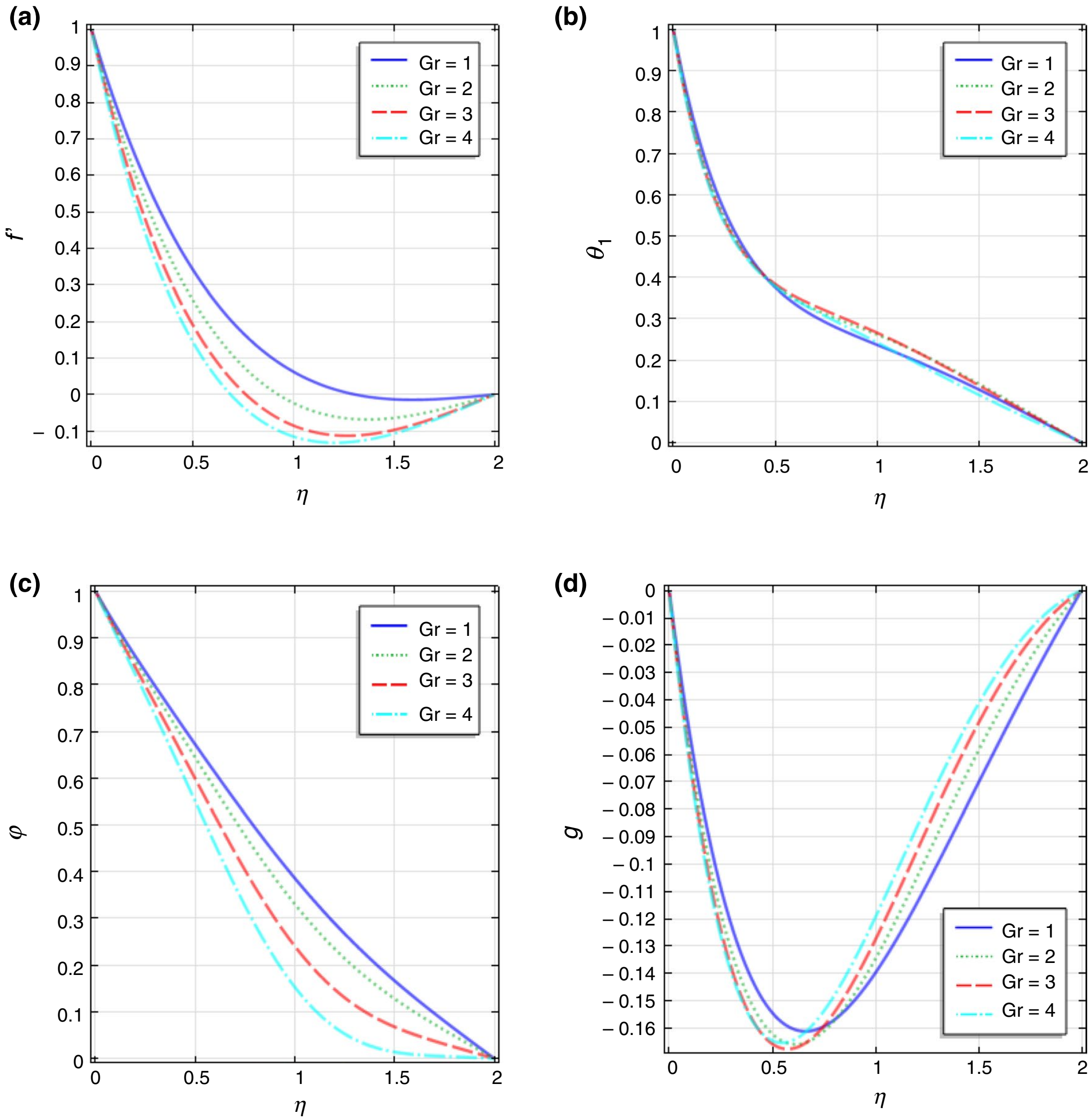

Fig. 4 **a** Velocity distribution, **b** temperature distribution, **c** concentration distribution, **d** angular velocity distribution for different values of Gr at $m_1 = 10, \phi_1 = 0.4, K = 0.2, \gamma_1 = 0.1, \mathrm{Gm} = 2, \beta = 0.1, \alpha_1 = 1, \mathrm{Pr} = 10, \lambda = 0.01, \varepsilon = 0.1, \mathrm{Nb} = 0.1, \mathrm{Nt} = 0.1, \chi = 2, Q_1 = 2, \mathrm{Sc} = 0.2, S = 0.1$

of thermal Grashof number. For increasing the values of thermal Grashof number decreases the velocity and concentration distributions. However, it enhances the temperature distribution. The thermal Grashof number favors the rotational velocity distribution. In case of ordinary viscous flow, thermal Grashof number increases the velocity and temperature distribution. Microrotation of the fluid and the rotation of the particles are also considered in this study. The rotation of the fluid particles in the fluid decreases the velocity distribution. Figure 5a–d indicate the velocity, temperature, concentration and angular velocity distribution for different values of thermal Solutal number. Increasing Solutal Grashof number increases the angular velocity distribution on the as shown in Fig. 5d. Solutal Grashof number favors the rotation of the magnetic fluid. It decreases the velocity distribution in ferrofluid. A decrease in the velocity distribution increases the thickness of boundary layer. However, the thermal boundary layer thickness increases for increasing values of Gm as shown in Fig. 5b.

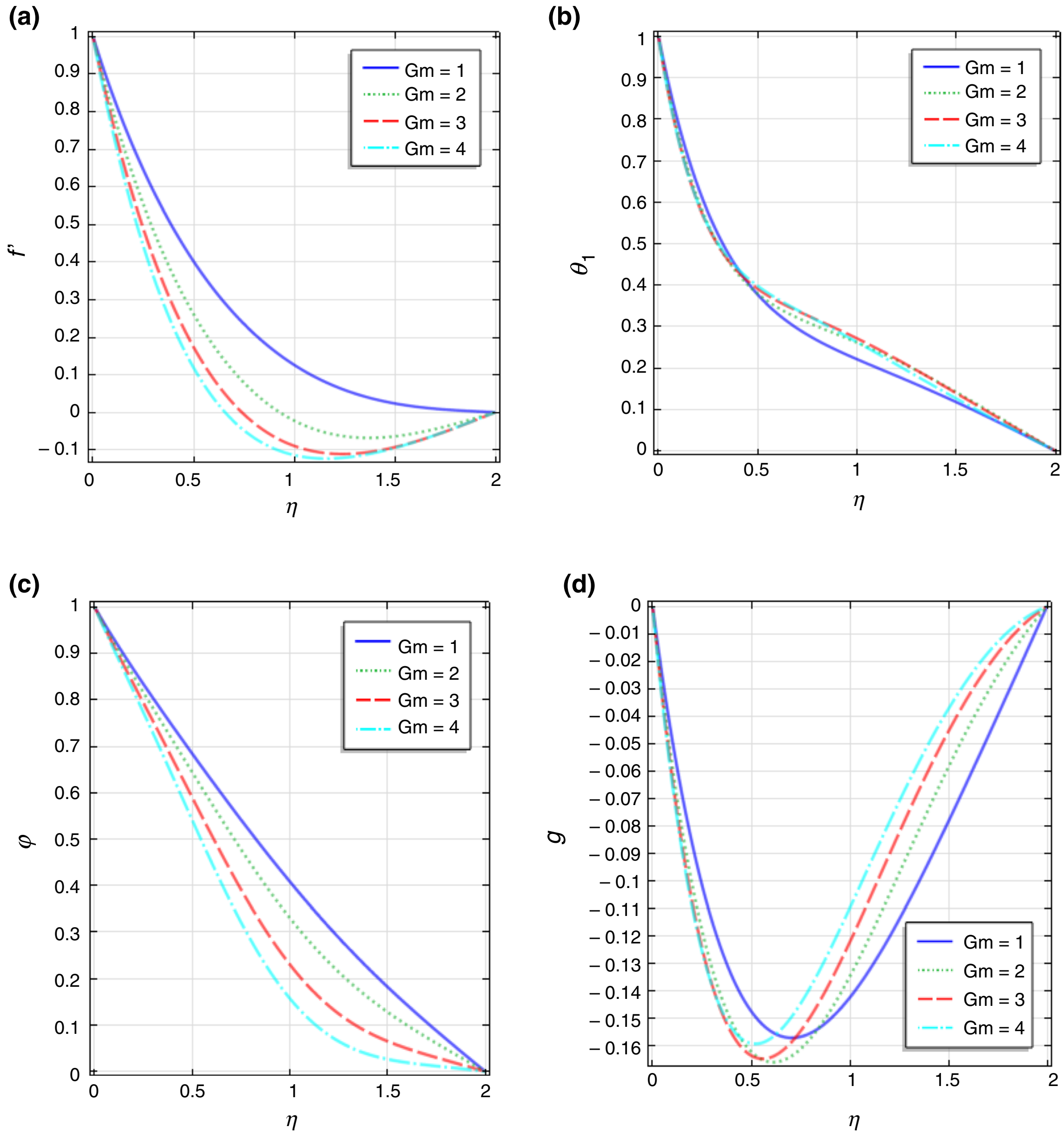

Fig. 5 **a** Velocity distribution, **b** temperature distribution, **c** concentration distribution, **d** angular velocity distribution for different values of Gm at $m_1 = 10$, $\phi_1 = 0.4$, $K = 0.2$, $\gamma_1 = 0.1$, $\mathrm{Gr} = 2$, $\beta = 0.1$, $\alpha_1 = 1$, $\mathrm{Pr} = 10$, $\lambda = 0.01$, $\epsilon = 0.1$, $\mathrm{Nb} = 0.1$, $\mathrm{Nt} = 0.1$, $\chi = 2$, $Q_1 = 2$, $\mathrm{Sc} = 0.2$, $S = 0.1$

Figure 6a–d represents the velocity, temperature, concentration and angular velocity distribution for different values of Brownian motion parameter Nb. Brownian motion parameter decreases the velocity distribution in the flow. Increasing the Brownian motion parameter enhances the angular velocity distribution. It happens in the presence of magnetic dipole. Magnetic field creates the additional viscosity in the fluid. Therefore, rotation of nanoparticles increases rather than velocity distribution. However, heat transfer and mass transfer increase for increasing values of Brownian motion parameter. Magnetic field plays an important role in changing heat and mass transfer characteristics in this flow. Figure 7a–d shows the velocity, temperature, concentration and angular velocity profiles for different values

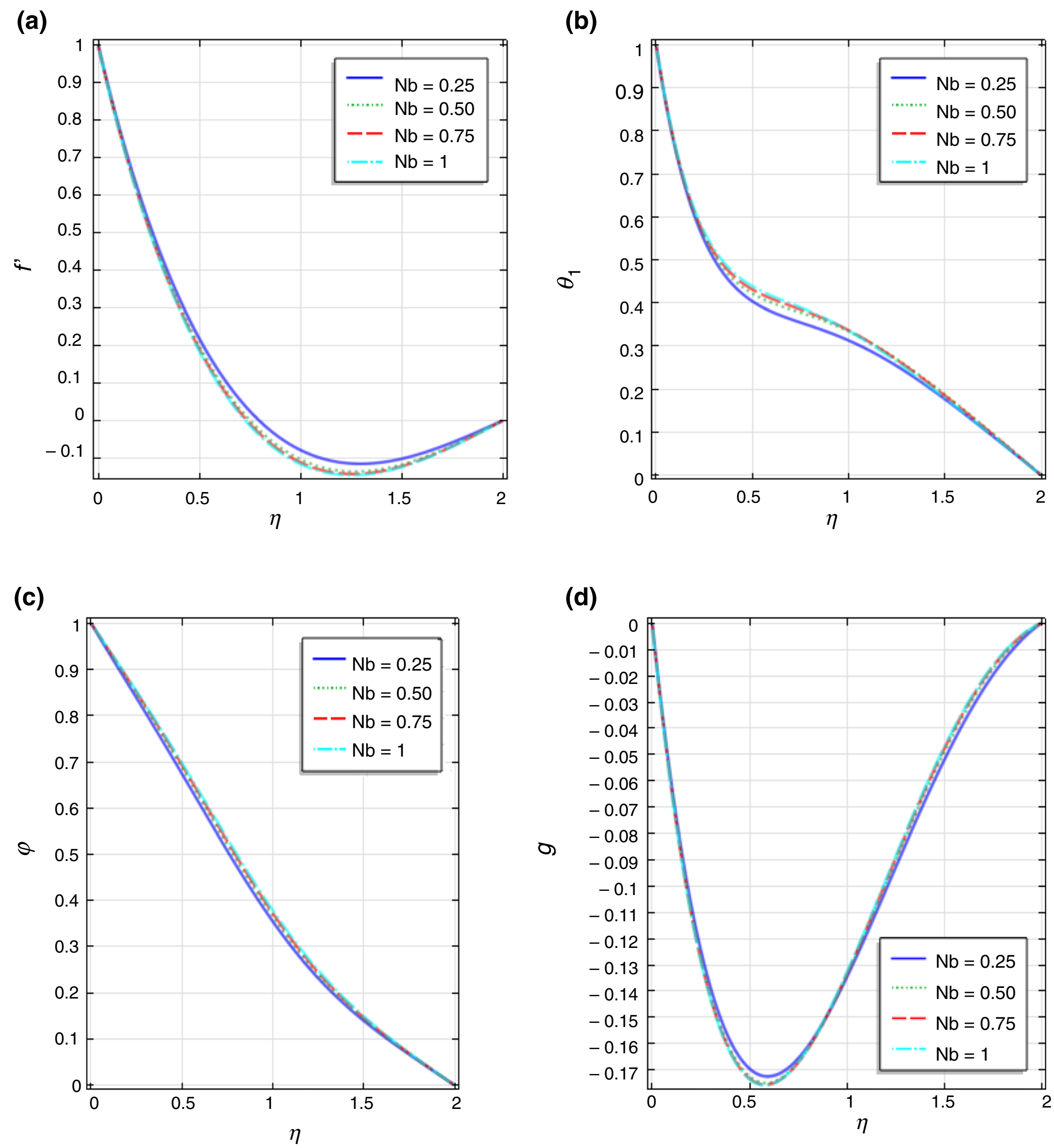

Fig. 6 **a** Velocity distribution, **b** temperature distribution, **c** concentration distribution, **d** angular velocity distribution for different values of Nb at $m_1 = 10$, $\phi_1 = 0.4$, $K = 0.2$, $\gamma_1 = 0.1$, $\mathrm{Gr} = 2$, $\beta = 0.1$, $\alpha_1 = 1$, $\mathrm{Pr} = 10$, $\lambda = 0.01$, $\varepsilon = 0.1$, $\mathrm{Gm} = 2$, $\mathrm{Nt} = 0.1$, $\chi = 2$, $Q_1 = 2$, $\mathrm{Sc} = 0.2$, $S = 0.1$

of thermophoresis parameter Nt. Increasing the values of thermophoresis parameter enhances the velocity distribution and reduces the angular velocity distributions. However, it decreases the heat transfer and concentration distribution in the ferrofluid flow.

Figure 8a–d represents the effect of chemical reaction parameter on the velocity, temperature, concentration and angular velocity distributions. Chemical reaction parameter in ferrofluid impedes the rotation of ferrofluids and speed up the velocity distribution. It also decreases the heat transfer and concentration distribution. Chemical reaction parameter has higher impact on mass transfer than heat transfer. Figure 9a, b depicts the effect of radiation parameter (Q_1) on the temperature and concentration

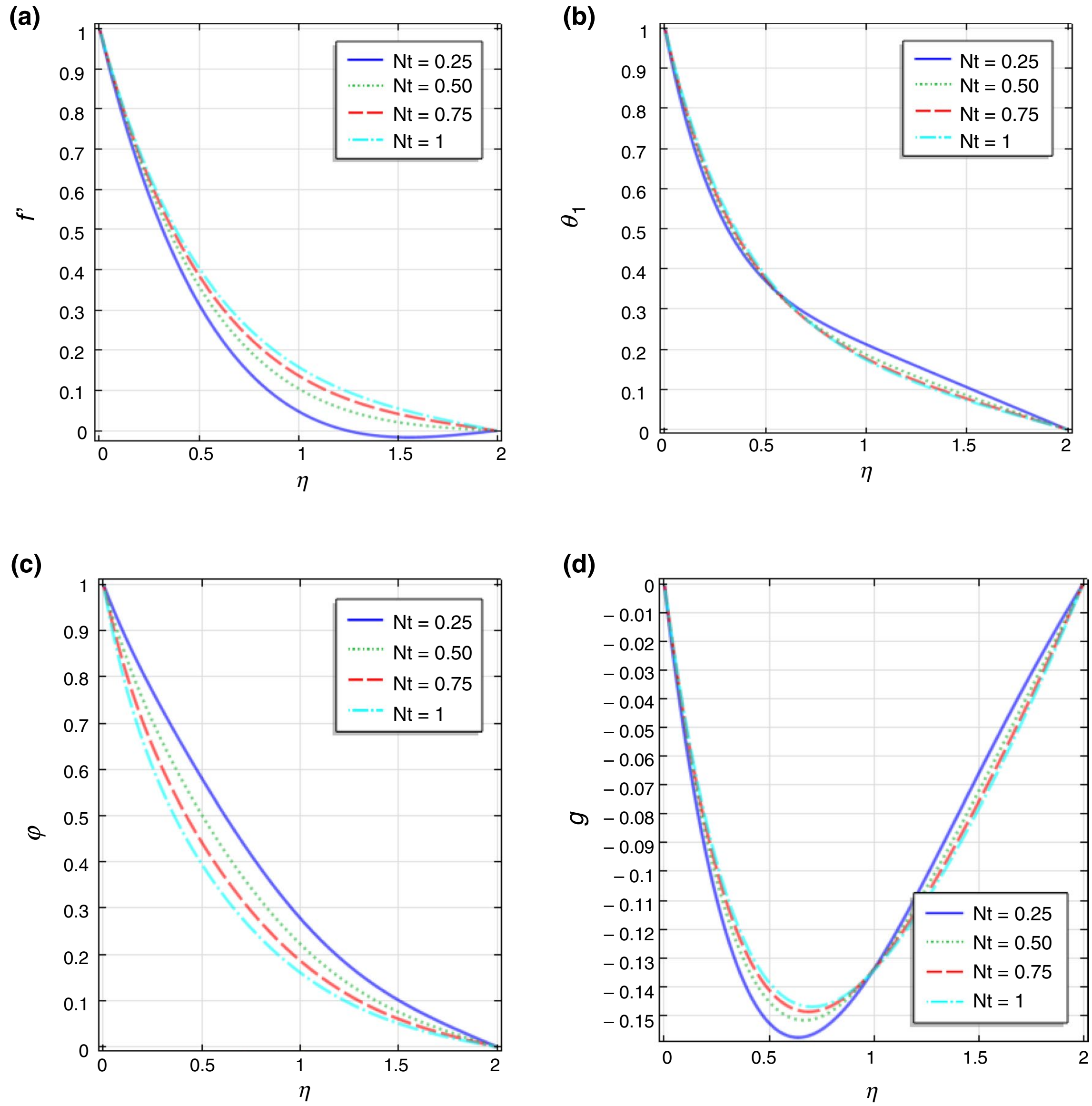

Fig. 7 **a** Velocity distribution, **b** temperature distribution, **c** concentration distribution, **d** angular velocity distribution for different values of Nt at $m_1 = 10$, $\phi_1 = 0.4$, $K = 0.2$, $\gamma_1 = 0.1$, $\mathrm{Gr} = 2$, $\beta = 0.1$, $\alpha_1 = 1$, $\mathrm{Pr} = 10$, $\lambda = 0.01$, $\varepsilon = 0.1$, $\mathrm{Gm} = 2$, $\mathrm{Nb} = 0.1$, $\chi = 2$, $Q_1 = 2$, $\mathrm{Sc} = 0.2$, $S = 0.1$

distributions. There is no significant impact of radiation parameter on the velocity and angular velocity distributions, and therefore these results are not presented in figures. However, increasing the radiation parameter increases the heat transfer distribution and decreases the concentration distribution. Figure 10a, b indicates the temperature and concentration distribution for different values of Prandtl number. The present results are obtained for different types of water-based ferrofluid. Increasing Prandtl number decreases the heat transfer distribution and increases the concentration in the fluid.

Figure 11a–d shows the velocity, temperature, concentration and angular velocity profiles for different values of heat absorption parameter χ. It increases the velocity distribution and decreases the angular velocity distribution in the flow. Increasing heat absorption parameter decreases the thermal

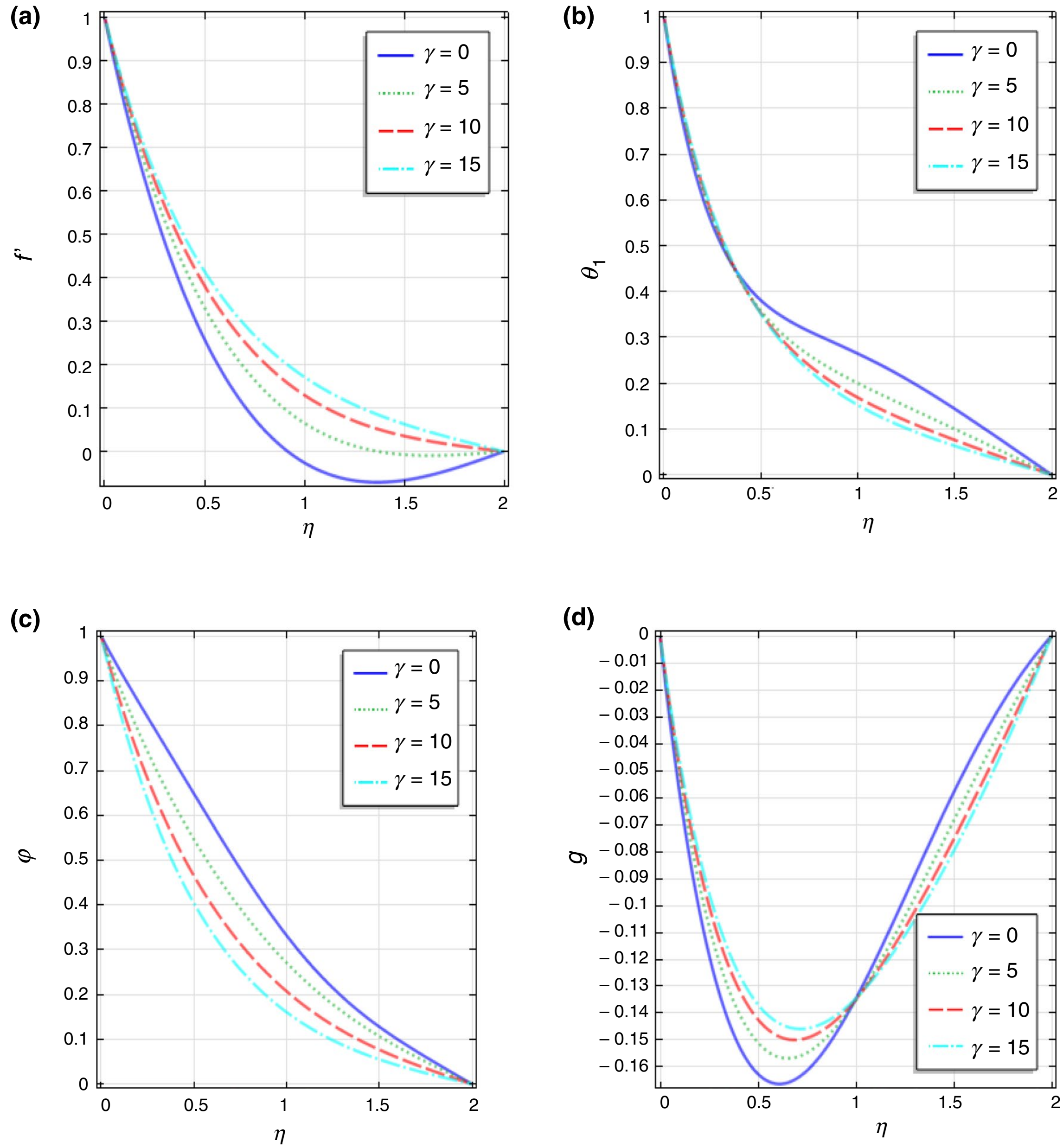

Fig. 8 **a** Velocity distribution, **b** temperature distribution, **c** concentration distribution, **d** angular velocity distribution for different values of γ at $m_1 = 10$, $\phi_1 = 0.4$, $K = 0.2$, $\gamma_1 = 0.1$, $\mathrm{Gr} = 2$, $\beta = 0.1$, $\alpha_1 = 1$, $\mathrm{Pr} = 10$, $\lambda = 0.01$, $\varepsilon = 0.1$, $\mathrm{Gm} = 2$, $\mathrm{Nb} = 0.1$, $\chi = 2$, $Q_1 = 2$, $\mathrm{Sc} = 0.2$, $\mathrm{Nt} = 0.1$, $S = 0.1$

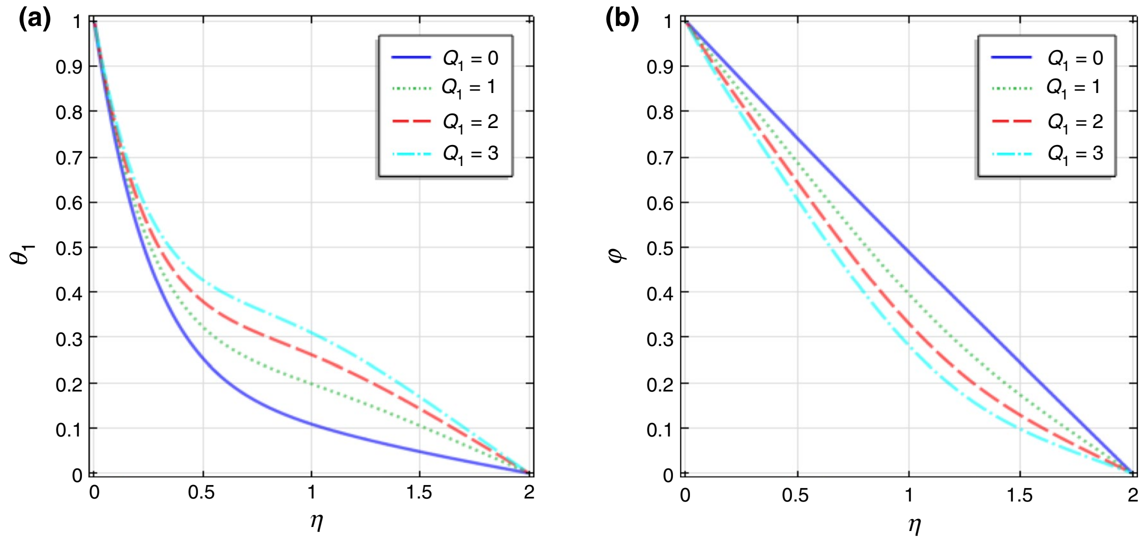

Fig. 9 **a** Temperature distribution, **b** concentration distribution for different values of Q_1 at $m_1 = 10$, $\phi_1 = 0.4$, $K = 0.2$, $\gamma_1 = 0.1$, $\mathrm{Gr} = 2$, $\beta = 0.1$, $\alpha_1 = 1$, $\mathrm{Pr} = 2$, $\lambda = 0.01$, $\varepsilon = 0.1$, $\mathrm{Gm} = 2$, $\mathrm{Nb} = 0.1$, $\chi = 2$, $\mathrm{Sc} = 0.2$, $\mathrm{Nt} = 0.1$, $\gamma = 2$, $S = 0.1$

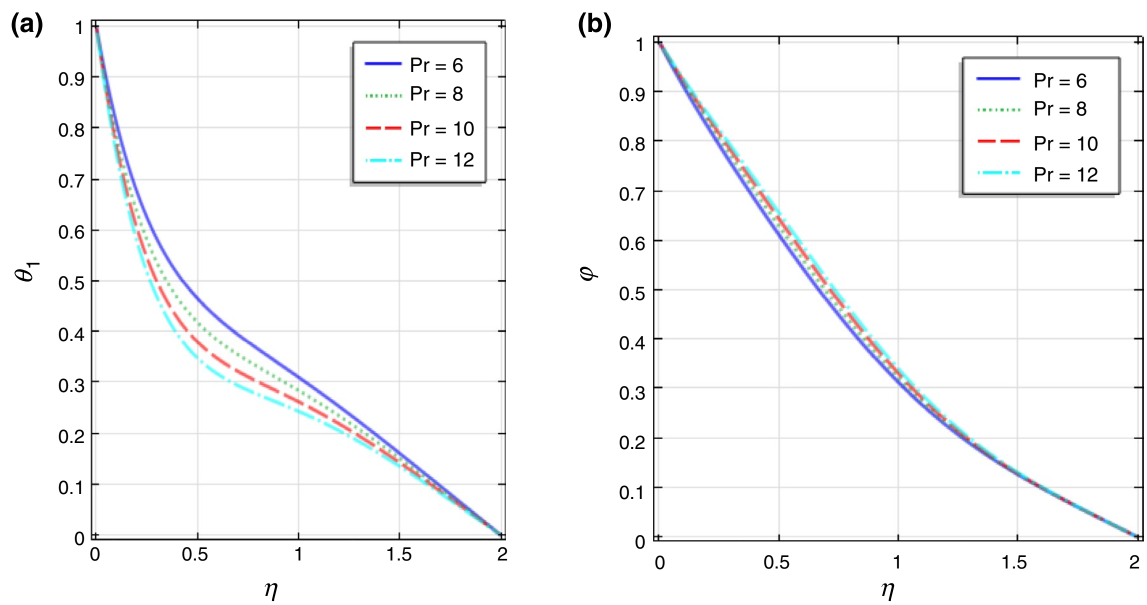

Fig. 10 **a** Temperature distribution, **b** concentration distribution for different values of Pr at $m_1 = 10$, $\phi_1 = 0.4$, $K = 0.2$, $\gamma_1 = 0.1$, $\mathrm{Gr} = 2$, $\beta = 0.1$, $\alpha_1 = 1$, $\mathrm{Sc} = 0.2$, $\lambda = 0.01$, $\varepsilon = 0.1$, $\mathrm{Gm} = 2$, $\mathrm{Nb} = 0.1$, $Q_1 = 2$, $\chi = 2$, $\mathrm{Nt} = 0.1$, $\gamma = 2$, $S = 0.1$

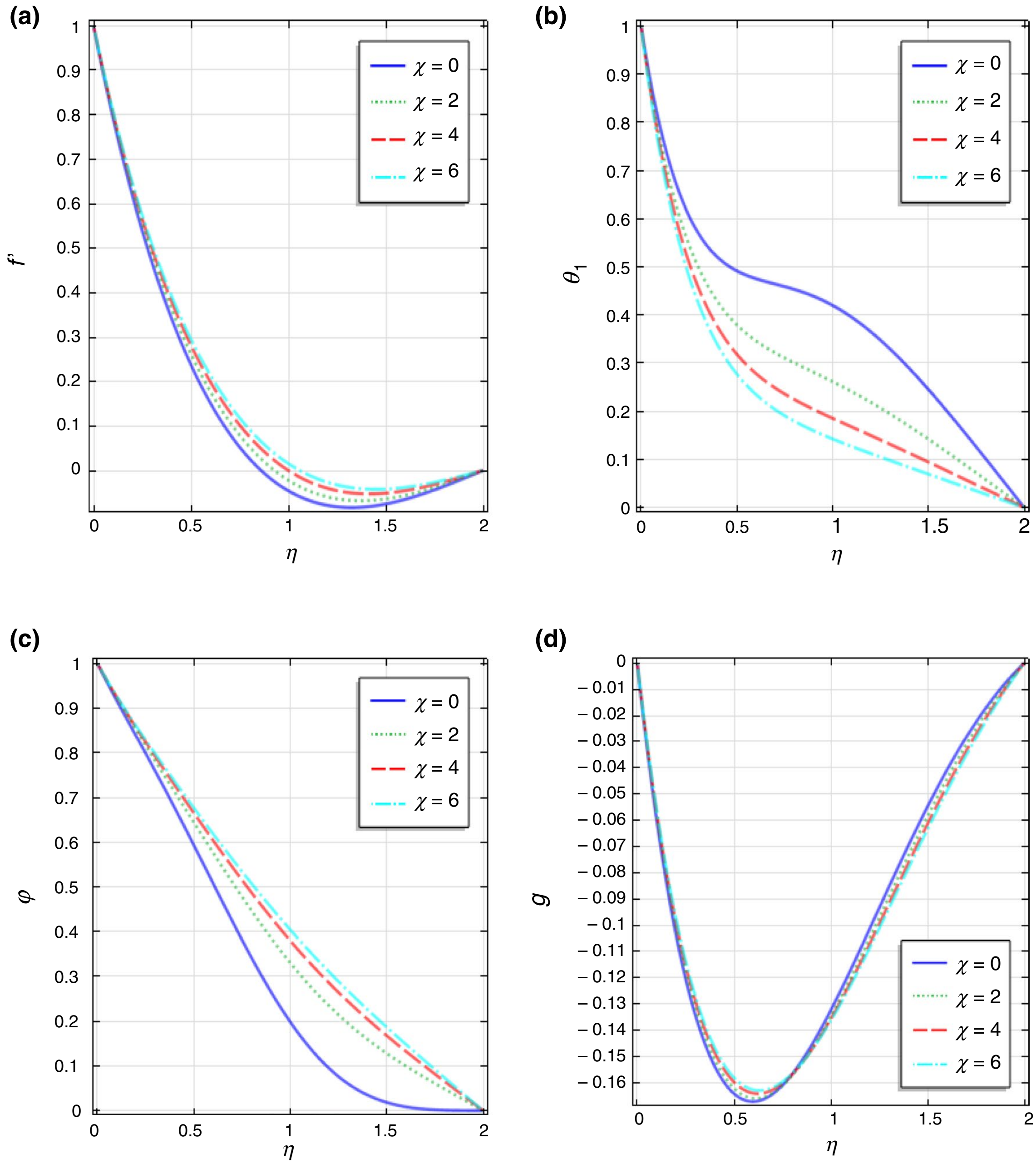

Fig. 11 **a** Velocity distribution, **b** temperature distribution, **c** concentration distribution, **d** angular velocity distribution for different values of, χ at $m_1 = 10$, $\phi_1 = 0.4$, $K = 0.2$, $\gamma_1 = 0.1$, $\mathrm{Gr} = 2$, $\beta = 0.1$, $\alpha_1 = 1$, $\mathrm{Pr} = 10$, $\lambda = 0.01$, $\varepsilon = 0.1$, $\mathrm{Gm} = 2$, $\mathrm{Nb} = 0.1$, $Q_1 = 2$, $\mathrm{Sc} = 0.2$, $\mathrm{Nt} = 0.1, \gamma = 2, S = 0.1$

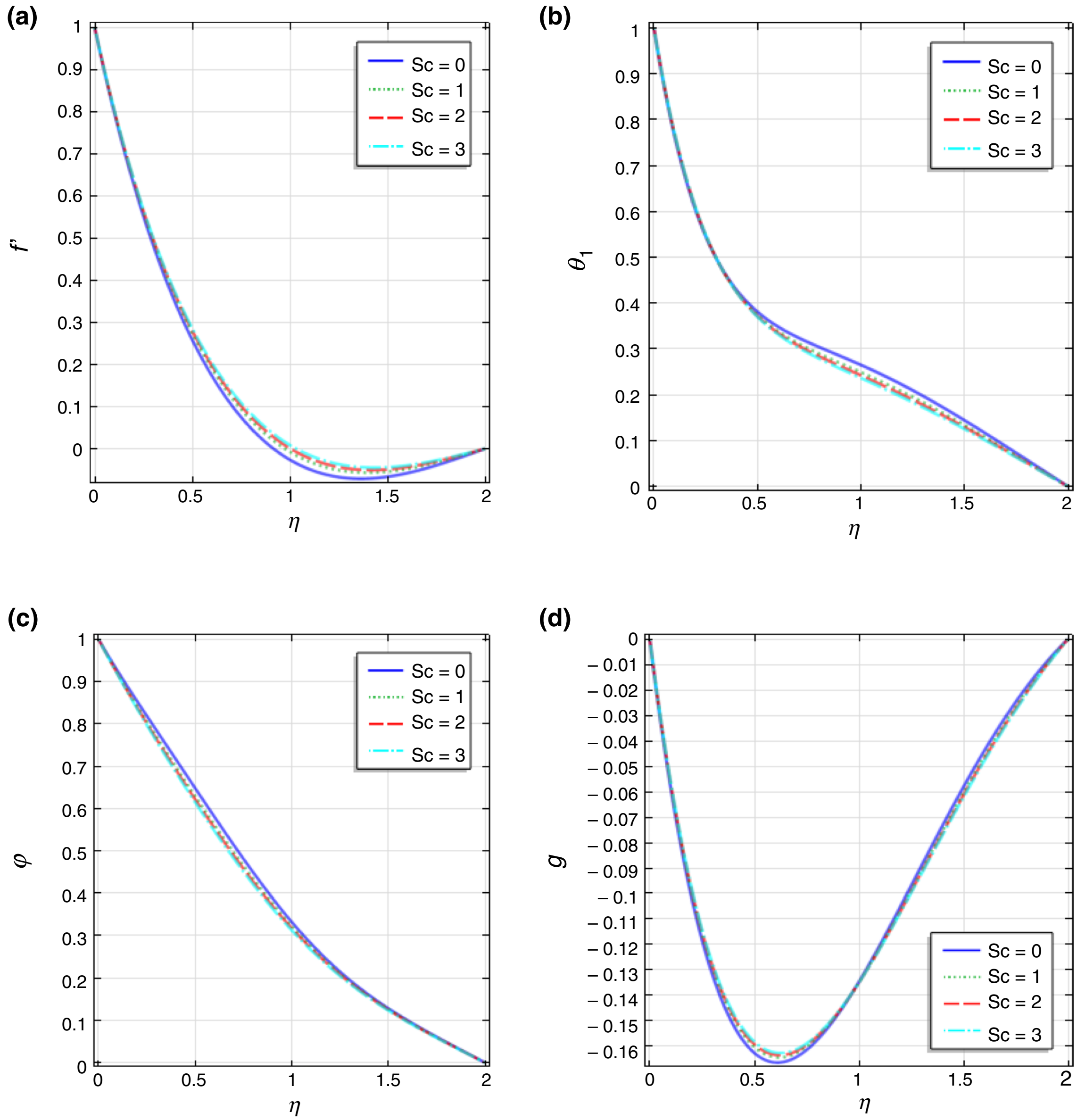

Fig. 12 **a** Velocity distribution, **b** temperature distribution, **c** concentration distribution, **d** angular velocity distribution for different values of Sc at $m_1 = 10$, $\phi_1 = 0.4$, $K = 0.2$, $\gamma_1 = 0.1$, Gr $= 2$, $\beta = 0.1$, $\alpha_1 = 1$, Pr $= 2$, $\lambda = 0.01$, $\varepsilon = 0.1$, Gm $= 2$, Nb $= 0.1$, $Q_1 = 2$, $\chi = 2$, Nt $= 0.1$, $\gamma = 2$

boundary layer thickness and increases the concentration boundary layer. This parameter transforms the thermal energy into concentration energy. Figure 12a–d shows the velocity, temperature, concentration and angular velocity profiles for different values of Schmidt number (Sc). In the current problem, the Schmidt has less impact on velocity, temperature, concentration and angular velocity distribution as compared to other physical parameter considered in the flow. In this flow, magnetization force, rotation of the nanofluid and rotational viscosity due to magnetic field play key role in changing the flow characteristics, heat transfer and mass transfer. The Schmidt number increases the velocity distribution and decreases the angular velocity of the ferromagnetic nanofluid. Far from the sheet, there is a small decrease in the heat and mass transfer in the considered flow.

Conclusions

In the present work, FHD nanofluid flow over a stretching surface considering the rotation of the particles has been investigated in the presence of a stationary magnetic field. The problem is solved through finite element method through COMSOL Multiphysics. Maxwell parameter, ferromagnetic interaction number, rotation of the fluid and rotational viscosity plays important role in velocity distribution, heat transfer and mass transfer. Physical parameter considered in FHD nanofluid flow has some interesting characteristics. Some important observations based on the present investigation for FHD flow are as follows:

- Increasing the values of ferromagnetic interaction number (β), Maxwell parameter $\left(\gamma_1\right)$, thermal Grashof number (Gr), solutal Grashof number (Gm) and Brownian motion Parameter (Nb) decreases the velocity distribution in the flow. However, for increasing values of thermophoresis parameter (Nt), chemical reaction parameter (γ) and heat absorption parameter χ increases the velocity distribution. When velocity decreases in the flow, some of the momentum force has been transformed into rotational force which increases the angular velocity distribution.
- Heat transfer in the magnetic fluid increases for increasing values of ferromagnetic interaction number, thermal Grashof number, solutal Grashof number, Brownian motion parameter and radiation absorption coefficient. It decreases for increasing the values of thermophoresis number, chemical reaction parameter, Prandtl number, heat absorption parameter and Schmidt number. However, concentration distribution increases only for increasing the values of Prandtl number and heat absorption parameter. For other parameters, the concentration decreases in the fluid.
- These results are presented in the composite effects of magnetization force, magnetic field-dependent viscosity and rotation of ferromagnetic fluid. Magnetic energy distributes into kinetic energy, thermal boundary layer and concentration boundary layer in the presence of considered physical parameters.

Compliance with ethical standards

Conflict of interest The authors declare that they have no conflict of interest.

References

1. Neuringer JL, Rosensweig RE. Ferrohydrodynamics. Phys Fluids. 1964;7:1927–37. https://doi.org/10.1063/1.1711103.
2. Neuringer JL. Some viscous flows of a saturated ferro-fluid under the combined influence of thermal and magnetic field gradients. Int J Non Linear Mech. 1966;1:123–37.
3. Andersson HI, Valnes OA. Flow of a heated ferrofluid over a stretching sheet in the presence of a magnetic dipole. Acta Mech. 1998;128:39–47.
4. Zeeshan A, Majeed A. Heat transfer analysis of Jeffery fluid flow over a stretching sheet with suction/injection and magnetic dipole effect. Alex Eng J. 2016;55:2171–81. https://doi.org/10.1016/j.aej.2016.06.014.
5. Salehpour A, Ashjaee M. Effect of different frequency functions on ferrofluid FHD flow. J Magn Magn Mater. 2019;480:112–31.
6. Zhao G, Wang Z, Jian Y. Heat transfer of the MHD nanofluid in porous microtubes under the electrokinetic effects. Int J Heat Mass Transf. 2019;130:821–30.
7. Rana P, Bhargava R. Numerical study of heat transfer enhancement in mixed convection flow along a vertical plate with heat source/sink utilizing nanofluids. Commun Nonlinear Sci Numer Simul. 2011;16:4318–34.
8. Yu W, France DM, Routbort JL, Choi SUS. Review and comparison of nanofluid thermal conductivity and heat transfer enhancements. Heat Transf Eng. 2008;29:432–60. https://doi.org/10.1080/01457630701850851.
9. Buongiorno J. Convective transport in nanofluids. J Heat Transf. 2006;128:240.
10. Sheikholeslami M, Rokni HB. Numerical simulation for impact of Coulomb force on nanofluid heat transfer in a porous enclosure in presence of thermal radiation. Int J Heat Mass Transf. 2018;118:823–31.
11. Sheikholeslami M, Arabkoohsar A, Ismail KAR. Entropy analysis for a nanofluid within a porous media with magnetic force impact using non-Darcy model. Int Commun Heat Mass Transf. 2020;112:104488.
12. Babazadeh H, Ambreen T, Shehzad SA, Shafee A. Ferrofluid non-Darcy heat transfer involving second law analysis: an application of CVFEM. J Therm Anal Calorim. 2020. https://doi.org/10.1007/s10973-020-09264-z.
13. Sheikholeslami M, Shehzad SA. Numerical analysis of Fe_3O_4–H_2O nanofluid flow in permeable media under the effect of external magnetic source. Int J Heat Mass Transf. 2018;118:182–92.
14. Daneshvar Garmroodi MR, Ahmadpour A, Hajmohammadi MR, Gholamrezaie S. Natural convection of a non-Newtonian ferrofluid in a porous elliptical enclosure in the presence of a non-uniform magnetic field. J Therm Anal Calorim. 2019. https://doi.org/10.1007/s10973-019-09045-3.
15. Ho CJ, Chen MW, Li ZW. Numerical simulation of natural convection of nanofluid in a square enclosure: effects due to uncertainties of viscosity and thermal conductivity. Int J Heat Mass Transf. 2008;51:4506–16.
16. Li Z, Sheikholeslami M, Chamkha AJ, Raizah ZA, Saleem S. Control volume finite element method for nanofluid MHD natural convective flow inside a sinusoidal annulus under the impact of thermal radiation. Comput Methods Appl Mech Eng. 2018;338:618–33.
17. Sudarsana Reddy P, Chamkha AJ, Al-Mudhaf A. MHD heat and mass transfer flow of a nanofluid over an inclined vertical porous plate with radiation and heat generation/absorption. Adv Powder Technol. 2017;28:1008–17.
18. Zubair Akbar M, Ashraf M, Farooq Iqbal M, Ali K. Heat and mass transfer analysis of unsteady MHD nanofluid flow through a channel with moving porous walls and medium. AIP Adv. 2016;6:045222. https://doi.org/10.1063/1.4945440.
19. Shahzad A, Ali R, Khan M. On the exact solution for axisymmetric flow and heat transfer over a nonlinear radially stretching sheet. Chin Phys Lett. 2012;29:084705.
20. Ali R, Shahzad A, Khan M, Ayub M. Analytic and numerical solutions for axisymmetric flow with partial slip. Eng Comput. 2016;32:149–54.
21. Ahmed J, Mahmood T, Iqbal Z, Shahzad A, Ali R. Axisymmetric flow and heat transfer over an unsteady stretching sheet in power law fluid. J Mol Liq. 2016;221:386–93.

22. Sheikholeslami M, Chamkha AJ. Flow and convective heat transfer of a ferro-nanofluid in a double-sided lid-driven cavity with a wavy wall in the presence of a variable magnetic field. Numer Heat Transf Part A Appl. 2016;69:1186–200. https://doi.org/10.1080/10407782.2015.1125709.
23. Khan M, Ali R, Shahzad A. MHD Falkner-Skan flow with mixed convection and convective boundary conditions. Walailak J Sci Technol. 2013;10:517–29.
24. Kim J, Kang YT, Choi CK. Analysis of convective instability and heat transfer characteristics of nanofluids. Phys Fluids. 2004;16:2395–401. https://doi.org/10.1063/1.1739247.
25. Hayat T, Khan MI, Imtiaz M, Alsaedi A, Waqas M. Similarity transformation approach for ferromagnetic mixed convection flow in the presence of chemically reactive magnetic dipole. Phys Fluids. 2016;28:102003. https://doi.org/10.1063/1.4964684.
26. Shahzad A, Ali R. Approximate analytic solution for magneto-hydrodynamic flow of a non-Newtonian fluid over a vertical stretching sheet. Can J Appl Sci. 2012;2(1):202–15.
27. Saedi M, Aminfar H, Mohammadpourfard M, Maroofiazar R. Simulation of ferrofluid flow boiling in helical tubes using two-fluid model. Heat Mass Transf und Stoffuebertragung. 2019;55:1–16. https://doi.org/10.1007/s00231-018-2400-9.
28. Kumar R, Raju CSK, Sekhar KR, Reddy GV. Three dimensional MHD ferrous nanofluid flow over a sheet of variable thickness in slip flow regime. J Mech. 2017;35:1–12.
29. Vatani A, Woodfield PL, Nguyen N-T, Dao DV. Thermomagnetic convection around a current-carrying wire in ferrofluid. J Heat Transf. 2017;139:104502.
30. Majeed A, Zeeshan A, Ellahi R. Unsteady ferromagnetic liquid flow and heat transfer analysis over a stretching sheet with the effect of dipole and prescribed heat flux. J Mol Liq. 2016;223:528–33.
31. Hayat T, Ahmad S, Khan MI, Alsaedi A. Exploring magnetic dipole contribution on radiative flow of ferromagnetic Williamson fluid. Results Phys. 2018;8:545–51.
32. Sokolov A, Ali R, Turek S. An AFC-stabilized implicit finite element method for partial differential equations on evolving-in-time surfaces. J Comput Appl Math. 2015;289:101–15.
33. Ram P, Bhandari A. Effect of phase difference between highly oscillating magnetic field and magnetization on the unsteady ferrofluid flow due to a rotating disk. Results Phys. 2013;3:55–60.
34. Ram P, Bhandari A, Sharma K. Effect of magnetic field-dependent viscosity on revolving ferrofluid. J Magn Magn Mater. 2010;322:3476–80.
35. Yasmeen T, Hayat T, Khan MI, Imtiaz M, Alsaedi A. Ferrofluid flow by a stretched surface in the presence of magnetic dipole and homogeneous–heterogeneous reactions. J Mol Liq. 2016;223:1000–5. https://doi.org/10.1016/j.molliq.2016.09.028.
36. Ghasemian M, Najafian Ashrafi Z, Goharkhah M, Ashjaee M. Heat transfer characteristics of Fe_3O_4 ferrofluid flowing in a mini channel under constant and alternating magnetic fields. J Magn Magn Mater. 2015;381:158–67.
37. Shliomis MI, Morozov KI. Negative viscosity of ferrofluid under alternating magnetic field. Phys Fluids. 1994;6:2855–61. https://doi.org/10.1063/1.868108.
38. Bacri JC, Perzynski R, Shliomis MI, Burde GI. Negative-viscosity effect in a magnetic fluid. Phys Rev Lett. 1995;75:2128–31. https://doi.org/10.1103/PhysRevLett.75.2128.

Publisher's Note Springer Nature remains neutral with regard to jurisdictional claims in published maps and institutional affiliations.